INSTITUTE OF PHYSICS PUBLISHING NANOTECHNOLOGY
Nanotechnology **17** (2006) 1454–1458 doi:10.1088/0957-4484/17/5/048

Strain relaxation and quantum confinement in InGaN/GaN nanoposts

Horng-Shyang Chen[1], Dong-Ming Yeh[1], Yen-Cheng Lu[1], Cheng-Yen Chen[1], Chi-Feng Huang[1], Tsung-Yi Tang[1], C C Yang[1], Cen-Shawn Wu[2,3] and Chii-Dong Chen[3]

[1] Graduate Institute of Electro-Optical Engineering and Department of Electrical Engineering, National Taiwan University, 1, Roosevelt Road, Section 4, Taipei, Taiwan, Republic of China
[2] Graduate Institute of Electro-Optical Engineering, National Taiwan University, Taiwan, Republic of China
[3] Institute of Physics, Academia Sinica, Taipei, Taiwan, Republic of China

E-mail: ccy@cc.ee.ntu.edu.tw

Received 16 November 2005, in final form 8 January 2006
Published 16 February 2006
Online at stacks.iop.org/Nano/17/1454

Abstract
Nanoposts of 10–40 nm top diameter on an InGaN/GaN quantum well structure were fabricated using electron-beam lithography and inductively coupled plasma reactive ion etching. Significant blue shifts up to 130 meV in the photoluminescence (PL) spectrum were observed. The blue-shift range increases with decreasing post diameter. For nanoposts with significant strain relaxation, the PL spectral peak position becomes less sensitive to carrier screening. On the basis of the temperature-dependent PL and time-resolved PL measurements and a numerical calculation of the effect of quantum confinement, we conclude that the optical behaviours of the nanoposts are mainly controlled by the combined effect of 3D quantum confinement and strain relaxation.

1. Introduction

Semiconductor nanostructures, particularly those of quantum nature, have been proved beneficial for enhancing light-emission efficiency. Among the various nanostructures, recently nanoposts and nanocolumns have attracted much attention because of their relatively simple fabrication procedures. Basically, two methods have been used for fabricating semiconductor nanoposts. In the top-down approach, electron-beam or other lithography and high-quality dry etching have been used for fabricating 30 nm InGaAs/InP nanoposts [1]. A 14 meV blue shift was observed for the nanoposts. Also, InGaN/GaN nanoposts 60–100 nm in diameter and 500 nm in height were fabricated with a special dry etching condition without using any lithography process [2]. A certain effect of 3D quantum confinement was observed at a low temperature. Meanwhile, by using anodic aluminium oxide nanoparticles as the etching mask and inductively coupled plasma reactive ion etching (ICP RIE), GaN nanoposts around 60 nm in size were produced [3]. Strain relaxation in such a structure was observed through microphotoluminescence and micro-Raman spectroscopy measurements.

In the bottom-up approach, the direct growth of nanoposts has been reported. With MBE, self-organized high-density GaN nanocolumns on sapphire substrate 53 nm in diameter were grown [4]. On the basis of a similar growth concept, InGaN/GaN nanocolumns on Si substrate, efficiently emitting light over the whole visible range, were recently reported [5]. Other similar growth accomplishments include InGaN nanoposts 2 μm in length and 70 nm in diameter on sapphire substrate grown with MO-HVPE [6], 150 nm InGaN nanoposts on Si substrate with MBE [7], and GaN nanoposts with AlGaN/GaN and AlN/GaN Bragg reflectors for forming a nanocavity on Si substrate, grown with MBE [8]. Photoluminescence (PL) and time-resolved photoluminescence (TRPL) measurements demonstrated the thermal stability of the optical properties of 70–90 nm InGaN nanoposts, indicating that quantum confinement plays a certain role in the optical properties of such a nanostructure [9].

With all these efforts, however, the optical properties of an InGaN/GaN quantum well (QW) nanopost have not been well studied yet. In particular, the relative importance of the effects of strain relaxation and 3D quantum confinement in an originally highly strained InGaN/GaN QW has not yet been well investigated, when such a QW structure is transformed

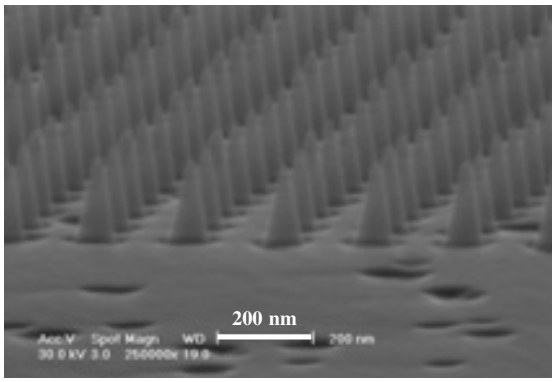

Figure 1. SEM image of the 10 nm nanoposts.

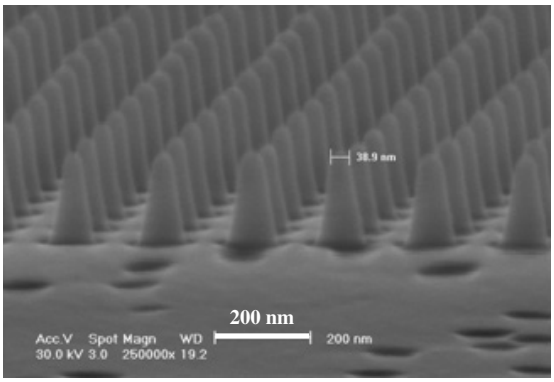

Figure 2. SEM image of the 40 nm nanoposts. The scale bar in the image shows a tip dimension of about 39 nm.

into a nanopost. In this paper, we report the fabrication of InGaN/GaN nanoposts and their optical characterization with a view to understanding the relative importance of the effects of strain relaxation and quantum confinement in such a nanopost. Nanoposts with diameter down to around 10 nm were fabricated using electron-beam lithography and ICP RIE on an InGaN/GaN QW structure. To the best of our knowledge, the 10 nm nanopost reported in this paper represents the thinnest pillar-shaped nanostructure on InGaN/GaN QW made with the top-down approach. From the PL and TRPL measurements, and a numerical calculation of the band structure, we find that the effects of strain relaxation and quantum confinement are both important in controlling the optical properties of such a nanostructure.

This paper is organized as follows. In section 2, we describe the nanopost fabrication procedures and the optical characterization methods. The geometries of the nanoposts are also shown in section 2 with scanning electron microscopy (SEM). The optical characterization results are reported in section 3. Then, a discussion of the importance of the effects of strain relaxation and quantum confinement is given in section 4. Finally, conclusions are drawn in section 5.

2. Fabrication procedures and optical characterization methods

The InGaN/GaN QW epi-structure was grown by metal–organic chemical vapour deposition. It consists of five pairs of 3 nm thick $In_{0.15}Ga_{0.85}N$ wells (grown at 710 °C) and 15 nm thick GaN barriers (also grown at 710 °C). The cap was a 20 nm GaN layer. The QW structure was grown on a 2 μm n-type GaN layer (grown at 1070 °C), which was grown on a (0001) sapphire substrate after a low-temperature-grown GaN buffer layer (25 nm, grown at 535 °C).

In fabricating the nanoposts, electron-beam lithography was used to define the nanosize hole patterns on a thin (∼200 nm) poly(methyl methacrylate) (PMMA) film. The energy and current of the electron beam were 30 keV and 25 pA, respectively. By controlling the exposure time, different dosages, leading to different patterned beam sizes, can be achieved. The dosages used were 10, 17, and 25 fC, corresponding to nanopost sizes of 10, 25, and 40 nm, respectively. After the electron-beam exposure, a 20 nm Cr film was deposited on the top. Then, the lift-off technique was used for producing a nanoscale Cr mask for chlorine-based ICP-RIE. The InGaN/GaN QW structure was etched to form the nanoposts. The etching conditions include Cl_2 (Ar) at 15 (20) sccm, bias power at 100 W, ICP source power at 200 W, chamber pressure at 5 mTorr, and etching time of 20 s. Under these etching conditions, we obtained nanoposts 180 nm in height. The top diameters of the nanoposts are around 10, 25, and 40 nm. For all the samples, the pitch is 200 nm.

Figure 1 shows an SEM image of a nanopost array with diameters of about 10 nm at the top. The post diameters increase from 10 nm at the top to about 25 nm at the bottom. In such a nanopost of changing diameter, the five InGaN/GaN QWs become quantum discs with diameters ranging from 11.7 to 17.7 nm. Figure 2 shows the SEM image of a nanopost array about 40 nm in diameter. The post diameter increases from 40 nm at the top to about 80 nm at the bottom. Therefore, the diameters of the five quantum discs vary from 44.4 to 60.4 nm.

For PL measurements, a HeCd laser of 325 nm was used for excitation. The laser was attenuated by a neutral density filter, partially reflected by a beam splitter, and then focused onto the sample through a long-working-distance objective of 0.45 numerical aperture. The spot size on the sample was estimated to be 1 μm in diameter. Under such excitation conditions, only 22 or fewer nanoposts were excited. The sample was placed in a liquid-helium-flow cryostat for low-temperature measurements. The luminescence of the nanoposts was collected by the objective, filtered with a long-wavelength-pass coloured glass, delivered through a fibre bundle, and finally analysed with a 0.5 m monochromator. For TRPL measurements, we used the second harmonic of a 100 fs Ti:sapphire laser at 730 nm for excitation. The optical measurement set-up was the same as that for the PL measurement. A streak camera system with a monochromator for the temporal and spectral domain measurements of the luminescence from the nanoposts was used. The temporal resolution of the system is 19 ps.

3. Optical characterization results

Figure 3 shows the PL spectra of the 10 nm, 40 nm nanoposts, and unpatterned samples, at room temperature with the excitation intensity at 0.4 W cm^{-2}. One can see that the PL spectral peaks of the 10 and 40 nm nanoposts blue

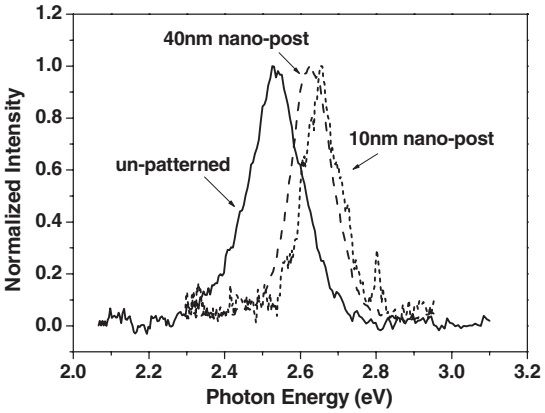

Figure 3. PL spectra of the 10 and 40 nm nanoposts, and the unpatterned sample, at room temperature when the excitation intensity is 0.4 W cm^{-2}.

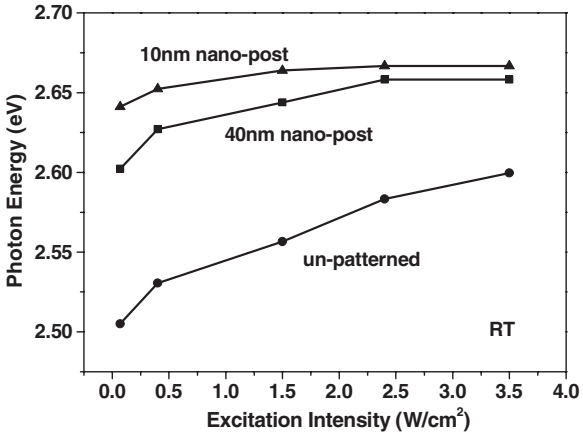

Figure 4. PL spectral shifts as functions of excitation intensity for the 10 and 40 nm nanoposts, and the unpatterned sample, at room temperature.

shift by 121.8 meV (22.5 nm) and 96.65 meV (18 nm), respectively, from those of the unpatterned sample. Also, the full width at half-maximum of the spectrum decreases with the post diameter, from 163.5 meV for the unpatterned sample to 118.6 meV for the 10 nm nanoposts. The blue shifts can be attributed to two causes: strain relaxation and quantum confinement. The trend of decreasing spectral width can be due to the reductions of the QW potential tilt and the range of indium composition fluctuation in the nanoposts.

The dependences of the PL spectral peak positions on the excitation intensity for the 10 nm, 40 nm nanoposts, and the unpatterned samples at room temperature, are shown in figure 4. Higher excitation intensity is expected to generate stronger effects of carrier screening and band filling, leading to a more significant blue shift in a particular sample [10, 11]. In the excitation intensity range up to 3.5 W cm^{-2}, the PL spectral peak of the unpatterned sample blue shifts by 94.5 meV (17.9 nm). However, the 40 nm (10 nm) nanopost sample peak blue shifts by only 55.8 meV (25.6 meV), which corresponds to 10 nm (4.5 nm). These results imply that the strain field originally in the QW is more relaxed in a nanopost of smaller diameter. However, the strain is not completely relaxed even when the quantum disc diameter is as small as 11–18 nm.

Figure 5 shows the temperature-dependent variations of the PL spectral peak positions of the 10, 25, 40 nm nanoposts, and the unpatterned sample. The excitation intensity is kept at 0.07 W cm^{-2}. A close examination leads to the conclusion of a general trend that a nanopost of smaller diameter has a smaller red shift with increasing temperature. This result could be due to the fact that the temperature dependence becomes weaker when the 3D quantum confinement is more significant.

Figure 6 shows the PL decay times of all these samples as functions of temperature, obtained from the TRPL measurements. The PL decay times were calibrated by fitting the time-resolved intensity profiles for the exponential decay time constants. One can see that the decay times generally decrease with temperature. The decreasing slope of the unpatterned sample is the steepest. The decay time increases with decreasing nanopost diameter. This variation trend is opposite to the effects of strain relaxation and quantum confinement. With strain relaxation, the overlap integral of

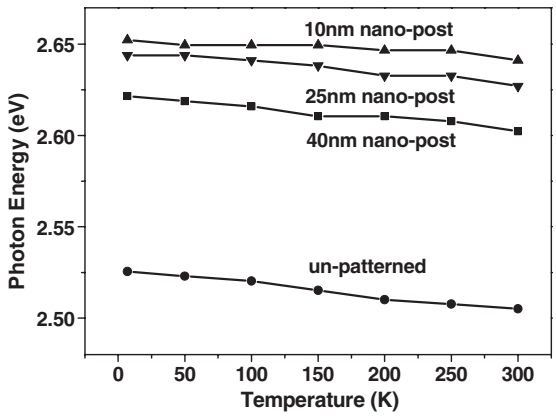

Figure 5. Temperature-dependent PL spectral peak positions of the 10, 25, and 40 nm nanoposts, and the unpatterned sample.

electron and hole is expected to be increased, leading to enhancement of the recombination rate and hence a reduction of the PL decay time. Also, with quantum confinement, recombination efficiency is increased and hence the PL decay time is reduced. Therefore, the increasing trend of the PL decay time with decreasing nanopost diameter requires other explanations (see section 4).

4. Discussion

Because of the large lattice mismatch between GaN and InN (up to 11%), a strong strain field exists in an InGaN/GaN QW structure. Also, the low miscibility of GaN and InN leads to indium compositional fluctuation and indium-rich nm-scale cluster formation in InGaN [12–14]. Such composition fluctuation and cluster structures are controlled by the strain condition in a QW [15]. The strain distribution results in a piezoelectric field and hence a potential tilt across a well layer that leads to a red shift of the emission spectrum and a reduction of the recombination efficiency. Such trends, called the quantum-confined Stark effect (QCSE), can be reversed when the strain is relaxed through nanopost

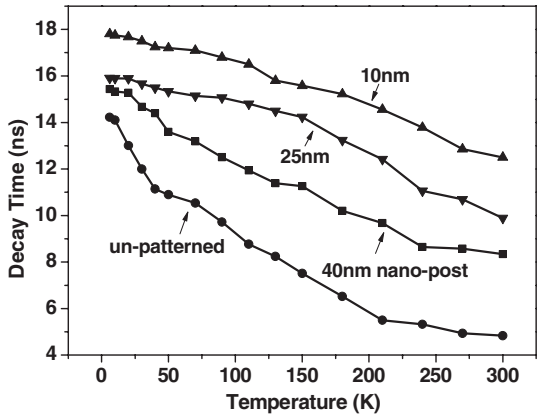

Figure 6. Temperature-dependent PL decay times of the 10, 25, and 40 nm nanoposts, and the unpatterned sample.

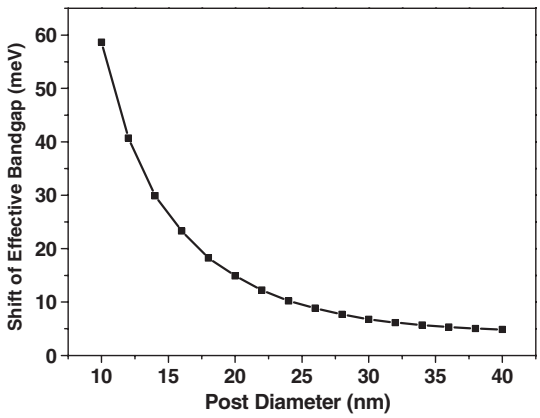

Figure 7. Calculation results for the blue shift of the effective band gap in a nanopost.

formation or the piezoelectric field is shielded through carrier screening [10, 11]. In a thinner post, strain relaxation is more significant and hence the range of its PL spectral blue shift is larger. In such a sample, the carrier screening effect becomes less effective in causing spectral shift, as demonstrated in figure 4.

Besides strain relaxation, the effect of quantum confinement also plays an important role in the optical behaviour of a nanopost. The dimensions of the InGaN regions in our nanoposts are actually comparable to those of the quantum dots grown with the Stranski–Krastanov mode [16, 17]. To estimate the effects of 3D quantum confinement in the nanoposts, we performed the numerical calculation for the effective band gap of an InGaN/GaN quantum disc 3 nm in thickness. Because of the infinite barrier potential (semiconductor/air) in the lateral direction, the 3D Schrödinger equation can be split into two equations for the lateral and the crystal growth dimensions. With azimuthal symmetry, the Schrödinger equation for the wavefunction, R, in the lateral dimension becomes

$$\rho^2 \frac{\partial^2 R}{\partial \rho^2} + \rho \frac{\partial R}{\partial \rho} + (\rho^2 - n^2)R = 0, \qquad (1)$$

which is a Bessel equation. Here, $\rho = k_0 r$, $k_0^2 = \frac{2mE}{\hbar^2}$, and n is the angular quantum number. Also, r is the radius in the cylindrical coordinate, m is the carrier mass, E is the energy state level, and $\hbar$ is Planck's constant divided by 2π. Considering the lowest energy state, we set $n = 1$. With the boundary condition, $R(k_0 a) = 0$, where a is the radius of the post, we can solve for k_0 and hence E. In the calculations, the following parameters were used: the indium composition is 15%, the effective electron mass of GaN (InN) is 0.176 421 m_0 (0.103 228 m_0), and the effective hole mass of GaN (InN) is 1.713 018 m_0 (1.639 008 m_0) [18]. Figure 7 shows the calculation results, which show that the effective band gap blue shifts by about 50 meV when the post diameter is 11 nm. This blue-shift value is not quite half the measured PL shift (about 130 meV) at low excitation, implying that the effect of strain relaxation plays an important role in the blue shifts of PL spectra. However, the effect of quantum confinement is also important.

In figure 3, we have shown that the PL spectral width decreases with decreasing post diameter. This trend is attributed to the reductions of the QW potential tilt and the range of indium composition fluctuation in the nanoposts. However, it is noted that the diameter variation of the quantum disc (11.7–17.7 nm for the 10 nm post and 44.4–60.4 nm for the 40 nm post) can contribute to PL spectral broadening. This contribution is particularly important for the 10 nm post because its quantum confinement effect is more significant. Therefore, the reduction of the spectral width in the nanopost is a combined effect of the reduction of the QW potential tilt, the decrease of the indium composition fluctuation, and the size variation of the quantum disc.

In figure 4, one can see that the differences in PL spectral peak position between the three samples decrease with increasing excitation intensity. For instance, between the 10 and 40 nm nanoposts, the difference is reduced from about 40 meV at low excitation to around 10 meV at the excitation intensity of 2.25 W cm^{-2}. The 40 meV difference at low excitation (see figure 4) is quite close to the about 35 meV difference from the contribution of quantum confinement (see figure 7). The proximity of the two numbers implies that the strain relaxation conditions of the 10 and 40 nm nanoposts can be about the same (but they are not fully relaxed yet). Therefore, the difference is mainly due to the quantum confinement. As the excitation intensity increases, a reduction of the QCSE occurs in both samples. However, the reduction for the 40 nm nanopost is more significant, leading to a shrinkage of the difference although the quantum confinement effects are quite different. The more significant reduction of the QCSE for the 40 nm nanoposts on increasing the excitation intensity is attributed to the smaller strain relaxation in this sample. With a stronger strain distribution, the QCSE is more significant and hence the effect of carrier screening is more prominent.

The only possible explanation for the increasing trend of the PL decay time with decreasing nanopost diameter is the reduction of non-radiative recombination after the nanoposts are fabricated. Because of the formation of quantum discs, carriers are well confined, away from the non-radiative centres, and the non-radiative recombination rate is tremendously reduced. This reduction dominates over the increasing trend of radiative recombination rate in forming nanoposts, leading to the decrease of the overall recombination

rate. Hence, the PL decay times increase with decreasing nanopost diameter. Because the decreasing trend of the PL decay time with increasing temperature is mainly due to the increasing contribution of non-radiative recombination, nanoposts of weaker non-radiative recombination are expected to have weaker temperature dependences on the PL decay time. Note that the effect of surface recombination in the nanoposts may play a certain role in the variation trends of the PL decay time. However, from the increasing trend of the PL decay time with decreasing nanopost diameter, it seems that the surface recombination is not a dominating factor here.

Similar research has led to a decreasing trend of PL decay time with nanopost diameter [19]. In this work, arrays of 50 and 100 nm posts were compared with an unpatterned sample. The indium composition of the InGaN/GaN QW epi-structure used was only 7%, which is significantly smaller than that for our samples. With the higher indium content in our samples, indium-rich clusters are normally formed [12]. The formation of such clusters is usually accompanied with the existence of stacking faults near the clusters [20]. In other words, the defect density becomes higher on increasing the indium content, as is the case for our samples. Hence, when the nanoposts were fabricated, the carrier confinement tremendously increased the PL decay time in our case. On the other hand, in [19] the dominating strain relaxation and quantum confinement led to a decrease of the PL decay time. It is noted that our PL decay times are still longer than those in [19]. This result is attributed to the contribution of carrier localization in our samples, which contain indium-rich clusters.

5. Conclusions

In summary, by using electron-beam lithography and ICP dry etching, nanoposts of 10–40 nm top diameter on an InGaN/GaN QW structure have been fabricated. Significant blue shifts in the PL spectra were observed. The blue-shift range increased with decreasing post diameter. For the nanoposts with significant strain relaxation, the PL spectral peak positions became less sensitive to carrier screening. From the temperature-dependent PL and TRPL measurements and a numerical calculation of the effect of quantum confinement, we concluded that the optical behaviours of the nanoposts were mainly controlled by the combined effect of 3D quantum confinement and strain relaxation.

Acknowledgments

This research was supported by National Science Council, The Republic of China, under the grants NSC 93-2210-M-002-006 and NSC 94-2215-E-002-015, and by the US Air Force, under the contracts AOARD-04-4026 and AOARD-05-4085.

References

[1] Temkin H, Dolan G J, Panish M B and Chu S N G 1987 *Appl. Phys. Lett.* **50** 413–5
[2] Hsueh T H, Huang H W, Lai F I, Sheu J K, Chang Y H, Kuo H C and Wang S C 2005 *Nanotechnology* **16** 448–50
[3] Wang Y D, Chua S J, Tripathy S, Sander M S, Chen P and Fonstad C G 2005 *Appl. Phys. Lett.* **86** 071917
[4] Yoshizawa M, Kikuchi A, Mori M, Fujita N and Kishino K 1997 *Japan. J. Appl. Phys.* **36** L459–62
[5] Kikuchi A, Kawai M, Tada M and Kishino K 2004 *Japan. J. Appl. Phys.* **43** L1524–6
[6] Kima H M, Kang T W and Chung K S 2004 *J. Ceram. Process. Res.* **5** 241–3
[7] Park Y S, Park C M, Fu D J, Kang T W and Oh J E 2004 *Appl. Phys. Lett.* **85** 5718–20
[8] Ristic J, Calleja E, Trampert A, Fernandez-Garrido S, Rivera C, Jahn U and Ploog K H 2005 *Phys. Rev. Lett.* **94** 146102
[9] Sun Y, Cho Y H, Kim H M and Kang T W 2005 *Appl. Phys. Lett.* **87** 093115
[10] Riblet P, Hirayama H, Kinoshita A, Hirata A, Sugano T and Aoyagi Y 1999 *Appl. Phys. Lett.* **75** 2241
[11] Choi C K, Kwon Y M, Little B D, Gainer G H, Song J J and Chang Y C 2001 *Phys. Rev.* B **64** 245339
[12] Lin Y S *et al* 2002 *Appl. Phys. Lett.* **80** 2571
[13] Feng S W, Cheng Y C, Chung Y Y, Yang C C, Lin Y S, Hsu C, Ma K J and Chyi J I 2002 *J. Appl. Phys.* **92** 4441
[14] Chen M K, Cheng Y C, Chen J Y, Wu C M, Yang C C, Ma K J, Yang J R and Rosenauer A 2005 *J. Cryst. Growth* **279/1-2** 55
[15] Cheng Y C *et al* 2004 *Appl. Phys. Lett.* **84** 2506
[16] Oliver R A, Andrew G, Briggs D, Kappers M J, Humphreys C J, Yasin S, Rice J H, Smith J D and Taylor R A 2003 *Appl. Phys. Lett.* **83** 755
[17] Kim H J *et al* 2004 *J. Cryst. Growth* **269** 95
[18] Chuang S L 1996 *IEEE J. Sel. Top. Quantum Electron.* **32** 1791
[19] Chen L, Yin A, Im J S, Nurmikko A V, Xu J M and Han J 2001 *Phys. Status Solidi* a **188** 135
[20] Lin Y S, Ma K J, Hsu C, Feng S W, Cheng Y C, Liao C C, Yang C C, Chuo C C, Lee C M and Chyi J I 2000 *Appl. Phys. Lett.* **77** 2988